Boundary-Layer Meteorol (2010) 137:271–290
DOI 10.1007/s10546-010-9531-y

ARTICLE

Evaluating a New Deposition Velocity Module in the Noah Land-Surface Model

U. Charusombat · D. Niyogi · A. Kumar · X. Wang · F. Chen · A. Guenther · A. Turnipseed · K. Alapaty

Received: 7 June 2009 / Accepted: 15 July 2010 / Published online: 4 August 2010
© Springer Science+Business Media B.V. 2010

Abstract The community Noah land-surface model (Noah LSM) has been modified to couple with a photosynthesis-transpiration scheme (GEM) to estimate the deposition velocity (V_d) for air quality studies. This new capability of the Noah-GEM model was tested in a point version of the National Center for Atmospheric Research-High Resolution Land Data Assimilation System (HRLDAS). Ozone V_d observations from June 1–30, 2002 over the AmeriFlux forested site located at Niwot Ridge, Colorado, USA (40°1′58″N; 105°32′47″W) were used. The model reasonably captures V_d variations for both dry and wet conditions but has problems at nighttime. Experiments were performed to assess the sensitivity of V_d calculations to surface characteristics related to vegetation and soil parameters. The results indicated that V_d values are sensitive to accurate specifications of the leaf area index (LAI) and a lesser extent to vegetation type, maximum stomatal resistance (R_{smax}) and soil texture prescription. The model sensitivity to canopy resistance was noted for both daytime and nighttime. For this forest site, neither soil textures nor soil moisture appeared to affect V_d calculations significantly, though they affected the surface heat-flux estimation particularly under low soil moisture conditions. Therefore, the V_d estimation in the Noah model can be enhanced by either site-specific LAI or assimilating regional normal difference vegetation index information for specific time periods. Results also highlighted the need to lower the current constant R_{smax} value used in Noah and other land-surface models.

U. Charusombat · D. Niyogi (✉)
Purdue University, West Lafayette, IN 47907, USA
e-mail: climate@purdue.edu

A. Kumar · X. Wang · F. Chen · A. Guenther · A. Turnipseed
National Center for Atmospheric Research, Boulder, CO 80307, USA

X. Wang
Sun Yat-Sen University, Guangzhou, China

K. Alapaty
DOE Atmospheric Radiation Measurement Program, Germantown, MD, USA

Keywords Air quality · Deposition velocity · Land data assimilation system · Noah land-surface model

1 Introduction

Regional models such as the Weather Research and Forecasting (WRF) model are widely applied for environmental and regional climate studies; WRF is also used for both operational weather and air quality forecasting (Grell et al. 2005). Land-surface models (LSM) such as the Noah LSM (Chen and Dudhia 2001; Ek et al. 2003) have been primarily used to develop realistic surface energy and water fluxes as surface boundary conditions for the WRF model. The land surface is also important as a sink for atmospheric pollutants through deposition pathways (Garland et al. 1974; Niyogi et al. 2003). In this paper, we discuss the development of a new capability for the Noah LSM, which will provide air-pollutant deposition velocity (V_d) estimates by coupling the Noah LSM with a photosynthesis-based canopy resistance formulation, referred to as the gas exchange evapotranspiration model (GEM).

Early understanding of V_d estimates was principally driven by field measurements and the synthesis of aerodynamic resistance (R_a), the boundary-layer resistance (R_b), and canopy resistance (R_c) (Garland et al. 1974; Wesely and Hicks 1977). Hicks et al. (1985) and Baldocchi et al. (1987) developed a resistance-based model to calculate V_d, and an enhancement of that modelling approach was adopted to include a multilayer model (MLM, Meyers et al. 1998; Cooter and Schwede 2000) to develop V_d estimates over the USA as part of the Clean Air Status and Trends Network (CASTNet) established by the US Environmental Protection Agency (EPA). While a number of other V_d model options exist (e.g. Erisman et al. 1994; Pleim et al. 2001; Zhang et al. 2003; Niyogi et al. 2003; Wu et al. 2009), this addition is used in developing a V_d module within Noah so as to use parts of these models to improve the description of atmosphere/land-surface interactions and to allow for gas exchange (particularly CO_2) fluxes in the coupled WRF-Chem/Noah model. Thus, the broader objective is to eventually develop capabilities for incorporating integrated environmental, hydrological, and surface energy balance/CO_2 flux studies using the Noah LSM as part of a land data assimilation system (Chen et al. 2007) or coupled WRF-Chem model. The existing option, Jarvis-type evapotranspiration schemes in the Noah LSM, does not have CO_2 interaction terms, and is heavily dependent on the minimum canopy resistance (R_{cmin}) specifications (Niyogi and Raman 1997; Niyogi et al. 2009). The evolving framework is being developed within the US National Science Foundation's BEACHON (Bio-hydro-atmosphere interactions of energy, aerosols, carbon, H_2O, and organics and nitrogen) initiative. Under the BEACHON framework, the Noah model is being modified to include the GEM canopy resistance scheme, which will then be linked with the model of emissions of gases and aerosols from nature (MEGAN) biogenic emission (Muller et al. 2008). These models will be fully integrated with the Noah LSM within the regional High Resolution Land Data Assimilation System (HRLDAS, Chen et al. 2007), WRF, and WRF-Chem. Thus, the ability of the Noah-GEM-HRLDAS framework to estimate V_d is of broad interest, and is the focus of this study.

The GEM-HRLDAS coupling has been discussed in Kumar et al. (2008), and the proof of concept tests for using GEM in air quality and land-surface studies has been reported in Niyogi et al. (2003, 2006) and Niyogi et al. (2006). Niyogi et al. (2009) developed and coupled the GEM to an atmospheric boundary-layer model and tested it over different landscapes. The photosynthesis-transpiration/stomatal resistance scheme showed good performance over different vegetation types. However, due to the big leaf approach used in the model, additional tests over forest canopies and heterogeneous soil moisture conditions are desired. The main

objectives of this study are, (i) to assess the performance of the Noah-GEM-HRLDAS model framework in calculating V_d over a forest site, and (ii) to assess the sensitivity of surface characteristics when calculating V_d.

In the following section, we discuss the experimental framework for the modelling experiments and the observational set-up. Section 3 presents the model results. The discussion first focuses on the performance of the modelling framework over the study site, while the subsequent discussion focuses on the sensitivity analysis of the model results to surface variables using different statistical approaches. Section 4 summarizes the conclusions.

2 Models and Site Description

2.1 Modelling Analysis

The Noah-GEM-HRLDAS was configured over the Niwot Ridge study site in Colorado, USA and initialized with static land use and soil texture fields as well as time-varying meteorological forcing fields. Single grid forcing data were created for the study period with 18 months of spin up from 1 Jan 2001–30 June 2002. Hourly meteorological forcing fields such as air temperature, surface mixing ratio, wind velocity components, and downward shortwave and longwave radiation fluxes were developed from the tower observations as input to the Noah model. For the 18-month period, precipitation fields were obtained from 4-km hourly NCEP (National Center for Environmental Prediction) stage-IV rainfall analysis, which is based on rain gage-calibrated WSR-88D radar (Weather Surveillance Radar 88 Doppler) rainfall estimates (Fulton et al. 1998). These calibrated rainfall fields over the Niwot site were morphed with onsite precipitation. The model was run as a single point HRLDAS system to develop offline estimates of V_d. The model calculates V_d as the inverse of the sum of the three resistance terms: R_a, R_b, and R_c. Different formulations can be used for estimating R_a, consequently we estimated R_a using onsite wind observations and the empirical approach of Lui et al. (2007). The R_b and R_c terms are computed in Noah-GEM following the photosynthesis approach (Niyogi et al. 2003, 2006); details of these formulations are given as Eqs. 8, 9, 10, and 11 in Appendix A. The model was run in a default mode with standard Noah and GEM parameters values. To assess the sensitivity of vegetation and soil parameters in the V_d estimation, 112 ensemble runs were performed (Table 1). Model results were analysed for changes in mean and diurnal patterns using time series and descriptive statistics. Furthermore, results were analysed to assess the impact of surface parameters on the V_d estimates using interaction explicit factorial analysis (Niyogi et al. 1999). The degree of agreement (d) and fractional bias (FB) between observation and model results were calculated using

$$d = 1 - \sum_{i=1}^{n} (o_i - m_i)^2 \Bigg/ \sum_{i=1}^{n} (|o_i| + |m_i|)^2 \,, \tag{1}$$

$$FB = 2\left(\frac{\sum_{i=1}^{n} o_i}{n} - \frac{\sum_{i=1}^{n} m_i}{n}\right) \Bigg/ \left(\frac{\sum_{i=1}^{n} o_i}{n} + \frac{\sum_{i=1}^{n} m_i}{n}\right), \tag{2}$$

where o_i is the observation, m_i is the model result, and n is the number of samples.

The periods of 7–12 June and 23–30 June 2002, which featured wet and subsequently dry soil conditions, are the focus of this paper. For 7–12 June 2002, the average soil moisture content was 15% due to 35 mm of accumulated precipitation during 3–5 June 2002. For 23–30

Table 1 Summary of experiments

Experiment	Variable	Values
Vegetation parameters		
1–4	Vegetation types	Deciduous needle leaf forest:12 Evergreen broad leaf forest:13 Evergreen needle leaf forest:14 Mixed forest:15
5–10	Leaf area index	1, 2, 3, 4, 5, 6
11–15	Green vegetation fraction	0.5, 0.6, 0.7,0.8, 0.9
16–20	Maximum stomatal resistance (s m^{-1})	1,000, 2,000, 3,000, 5,000, 7,500
Soil textures		
21–32	Texture	Sand, loamy sand, sandy loam, silt loam, silt, loam, sandy clay loam, silty clay loam, clay loam, sandy clay, silty clay, and clay.
Soil properties		
33–40	Hydraulic function	±10%, ±25%, ±50%, ±100%
41–48	Saturated soil metric potential	±10%, ±25%, ±50%, ±100%
49–56	Albedo	±10%, ±25%, ±50%, ±100%
57–64	Roughness length	±10%, ±25%, ±50%, ±100%
65–72	Dry soil moisture content	±10%, ±25%, ±50%, ±100%
73–80	Maximum soil moisture content	±10%, ±25%, ±50%, ±100%
81–88	Reference soil moisture content	±10%, ±25%, ±50%, ±100%
89–96	Soil hydraulic conductivity	±10%, ±25%, ±50%, ±100%
97–104	Saturated soil water diffusivity	±10%, ±25%, ±50%, ±100%
103–112	Quartz content	±10%, ±25%, ±50%, ±100%

June 2002, the accumulated precipitation was 6 mm with the average soil moisture content of 8.8%. Figure 1 shows the time series of observed precipitation, soil moisture, and V_d values for June 2002. According to Turnipseed et al. (2009), the V_d values generally increased after rainfall due to chemical reactions on the leaf surface.

2.2 The Niwot Ridge Site

The Niwot Ridge AmeriFlux site (40°1′58″N; 105°32′47″W) is located in the Roosevelt National Forest in the Rocky Mountains of Colorado, USA and is dominated by a subalpine forest with an abundance of Lodgepole pine, Engelmann spruce, and subalpine fir (Turnipseed et al. 2009). The study period for the V_d analysis was June 2002 because of the higher summer time ozone concentrations over the study region. The site has peak ozone concentrations when the upslope flow carries pollutants from the Denver metropolitan area, which typically occurs during the late afternoon and early evening periods. Turnipseed et al. (2006, 2009) characterized the Niwot Ridge site with a leaf area index (LAI) of 4.2 and roughness length of 1.6 m; the typical canopy height is 11.4 m and displacement height is 7.8 m.

The Niwot Ridge site is an active AmeriFlux site and has a variety of instruments to estimate surface atmosphere exchanges. Data are typically available at 15-min or 30-min intervals; as a result, the deposition velocities (V_d) were estimated as a ratio of deposition flux and

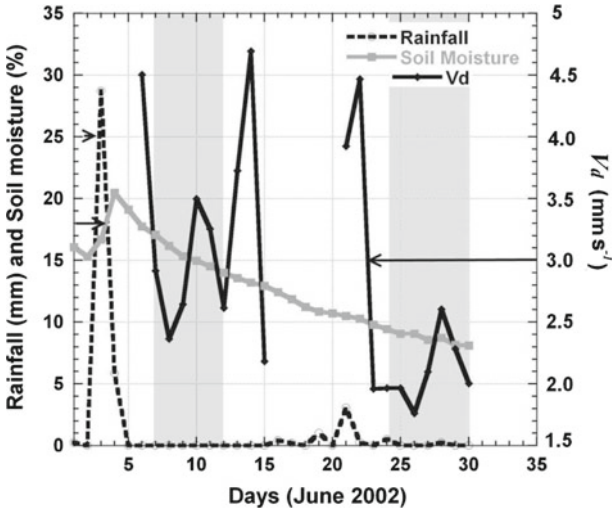

Fig. 1 Observed rainfall, percent of soil moisture at 0.01 m, and dry deposition velocity, V_d, during June 2002. The shaded boxes correspond to the "wet" and "dry" periods analysed in the study

gas concentration. The fluxes were calculated using the eddy-covariance technique, and gas concentrations were measured by an ultraviolet absorption ozone monitor (Turnipseed et al. 2009). Other parametric values, particularly the resistance terms used for model comparison, are calculated using onsite meteorological and V_d observations along with the back calculation of aerodynamic and boundary-layer resistances following Hicks et al. (1987). Additionally, the canopy resistance was calculated using a Penman-Monteith resistance formulation (Turnipseed et al. 2003; Alfieri et al. 2008 also see Lamaud et al. 2002). Other micrometeorological quantities (radiation fluxes, surface meteorology, and soil parameters/variables) required for driving the offline HRLDAS (Chen et al. 2007) were compiled from onsite observations.

3 Results and Discussion

Study results are presented in five sections. First, the comparison of the Noah-GEM-HRLDAS model results with field observations is discussed, which is followed by an ensemble analysis of the sensitivity of V_d to different surface parameters. The sensitivity of V_d estimation is further discussed using a factorial analysis and a two-factor interaction analysis approach. The final discussion addresses the impact on the model's performance when modifications are made to significant variables identified by sensitivity analysis.

3.1 Evaluating Noah-GEM V_d Estimates

The model results shown in Figs. 2, 3, 4, and 5 were obtained from a simulation with the default values of parameters in Noah-GEM-HRLDAS representative of a forest site. Figure 2 shows the observed and simulated ozone V_d values for 7–12 June 2002 (wet) and 23–30 June 2002 (dry) periods. The model slightly underestimated V_d for wet to moderate surface conditions for 7–12 June 2002, though it captured the day-to-day variability well. The model could not capture the high V_d values (14.2 and 11.7 mm s^{-1}) in the afternoon after rain events

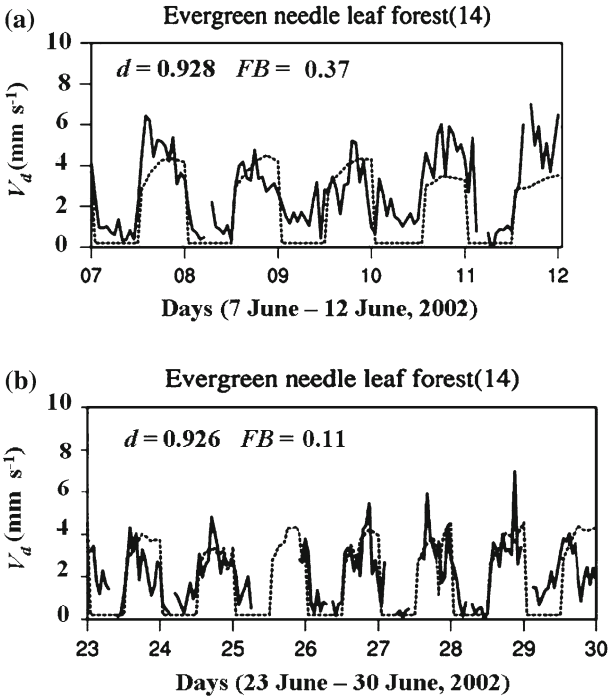

Fig. 2 Dry deposition velocity, V_d, time series for $LAI = 4$. *Solidline* represents observations and *dashedline* is the model estimates. **a** The period 7–12 June 2002 was relatively wet. **b** The period 23–30 June 2002 corresponds to a relatively dry period. The variable, *d*, is the index of agreement and *FB* is the fractional bias ($\mathrm{mm\,s^{-1}}$)

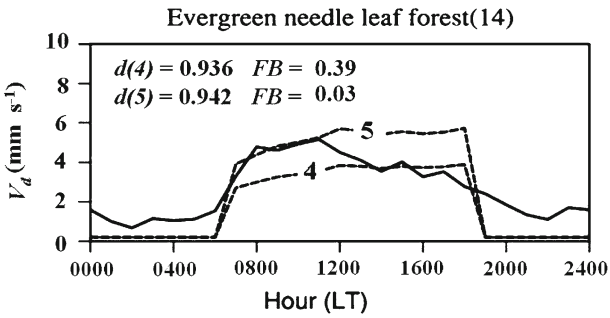

Fig. 3 Average diurnal dry deposition velocity V_d for June 2002 over the Niwot Ridge study site. *Solidline* indicates observations. *Dashedlines* correspond to model results. The index of agreement is *d*; FB is the fractional bias ($\mathrm{mm\,s^{-1}}$) with the LAI of 4 and 5

on June 6, 2002 (not shown). Turnipseed et al. (2009) also noted this increase in V_d after rain both as a possible impact of moist leaves leading to additional chemical interactions and as possible meteorological and non-stomatal feedbacks. The chemical interactions are currently not represented in the model. Under anomalously dry soil moisture conditions, the model is able to realistically capture the midday peak values and the diurnal variations in V_d. This is

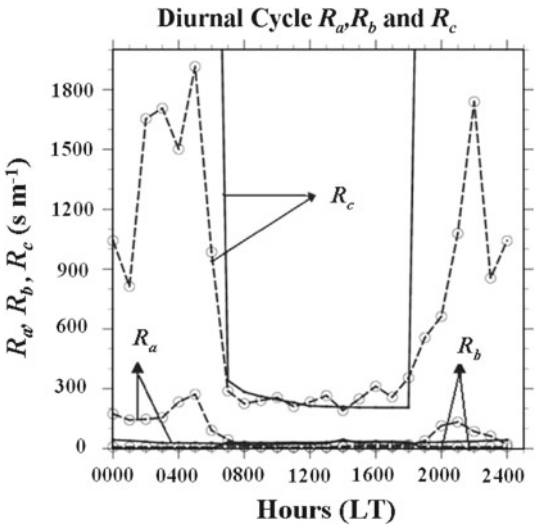

Fig. 4 The average diurnal aerodynamic resistance (R_a), boundary-layer resistance (R_b), and canopy resistance (R_c) for June 2002 over the Niwot Ridge study site. *Open circles with dashedline* are observations. *Solidlines* correspond to model results. Model R_c values for 0000–6000 and 1800–2400 LT have been set to maximum stomatal resistance (R_{smax}) measured as 5, 000 s m^{-1}

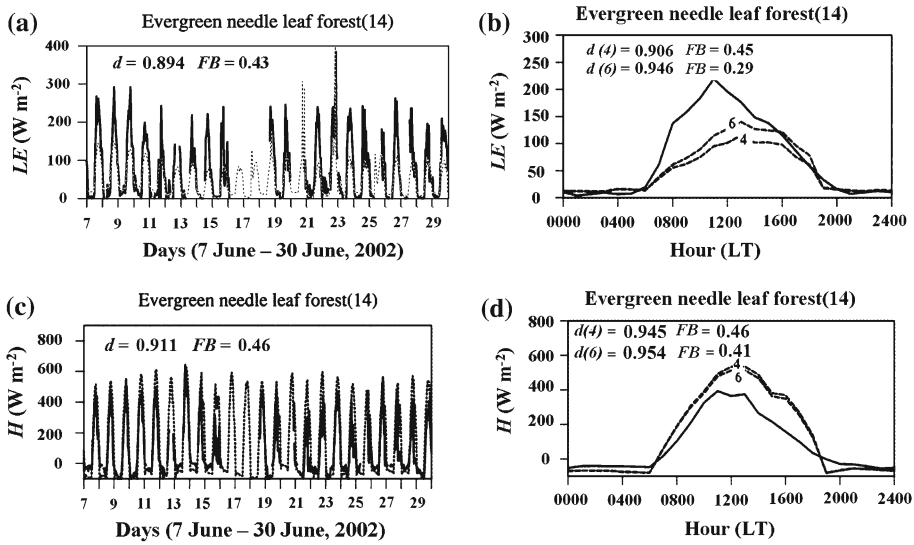

Fig. 5 **a** Latent heat flux (*LE*) and **c** sensible heat flux (*H*) plots for 7–30 June 2002 **b** and **d** average diurnal *LE* and *H* for 7–30 June 2002 over the Niwot Ridge study site. *Solidline* represents observations; *dashedline* represents model values. The period from 7–12 June 2002 was relatively wet while 23–30 June 2002 period corresponds to a relatively dry period. The term *d* is the index of agreement while *FB* is the fractional bias (W m^{-2}) with $LAI = 4$ and 6

reflected in the model index of agreement (d) and bias (FB) statistics for the wet and dry periods as 0.93 ± 0.37 and 0.93 ± 0.11 mm s^{-1}, respectively (Fig. 2).

Figure 3 shows the average diurnal V_d variation for model simulations using different LAI values. When using $LAI = 4$ (the default in Noah), the model underestimated the morning and nighttime V_d values, but changing LAI values to 5 agreed better with daytime and early afternoon observations. For nighttime conditions, the model's V_d values quickly fell to near zero while the observations showed values around 1.5–2 mm s^{-1}. While the modelled V_d

values were calculated as the sum of R_a, R_b and R_c, the mean diurnal variation of these resistances was also analysed (Fig. 4). Consistent with prior observations, R_c was the dominant term giving values one to two orders of magnitude higher than R_a and R_b. The model produced slightly lower than observed R_a, R_b, and R_c values during daytime. The Noah LSM estimated R_c value was notably different from the nighttime observations. In particular, the late evening dip in the model V_d values appeared to be related to an increased R_c in the Noah estimates. R_c increased in response to cooling after sunset, and the observed R_c was smaller than the constant value (5,000 s m^{-1}) assumed in the model, and may be due to sporadic night transpiration in response to vapour pressure deficit and air temperature changes (Musselman and Minnick 2000; Cavender-Bare et al. 2007; Kavanagh et al. 2007; Fisher et al. 2007).

Since R_c also affects the surface energy balance (Niyogi and Raman 1997), the modelled and observed latent (*LE*) and sensible heat fluxes (*H*) were also evaluated. The model underpredicted *LE* while *H* was in good agreement (Fig. 5). The model accurately identified most of the peaks in *LE* but missed the late afternoon values particularly for the dry period (Fig. 5a, b). Similar results were seen for the sensible heat flux (Fig. 5c, d). The diurnal peaks of *LE* were also shifted as compared to the observations. However, there are high uncertainties in both measuring and modelling latent heat fluxes. Because of the response of canopy resistance and the latent heat flux feedback, it appears that the model results were greatly affected by radiation. This may explain the underestimation of the high latent heat flux in the morning and afternoon hours. Furthermore, a dew related feedback, which is not accounted for in the model, may also be in action along with additional uncertainties in the model parameters. Further LAI calibrations could not overcome these mismatches.

To further diagnose the impact of surface parameters on the model performance, an ensemble sensitivity assessment was undertaken, which is discussed in the following sections.

3.2 Sensitivity of V_d to Soil and Vegetation Parameters

The Noah-GEM model parameters were systematically altered as documented in Table 1. First, the vegetation parameters were changed one at time, involving changing the vegetation type while maintaining other parameters in their default setting. Then, for the rest of the experiments, the vegetation type was fixed to type 14 (evergreen needle leaf forest for the study site) and the other variables were modified. For example, LAI was changed from 1 through to 6, after which LAI was set to the default value and the green vegetation fraction was changed from 0.5 through to 0.9 in increments of 0.1. The green vegetation fraction was then set back to default and the maximum stomatal resistance (R_{smax}) value was modified from 1,000 to 7,500 s m^{-1}, as shown in Table 1. The corresponding changes in the model simulated V_d were analysed. After assessing the sensitivity of the vegetation parameters, these parameters were reset to default values and the soil texture parameters were then changed to test the model's sensitivity. For example, the vegetation type was changed from 14 (default) to 13, then before changing the soil parameter, the vegetation type must be changed back to the default value (14). For these cases, the model was run for every soil texture while other values were retained at default. Following this, the sensitivity of individual soil properties was considered while the soil texture was set to default. The values and the experiments are listed in Table 1.

Figure 6a shows the V_d variation for the four different vegetation types. The V_d values increased when the vegetation type was changed from evergreen needle leaf forest to deciduous needle leaf forest and mixed forest. Evergreen needle leaf forest also had the lowest V_d variations. The V_d values over mixed and deciduous needle leaf forest ranged from

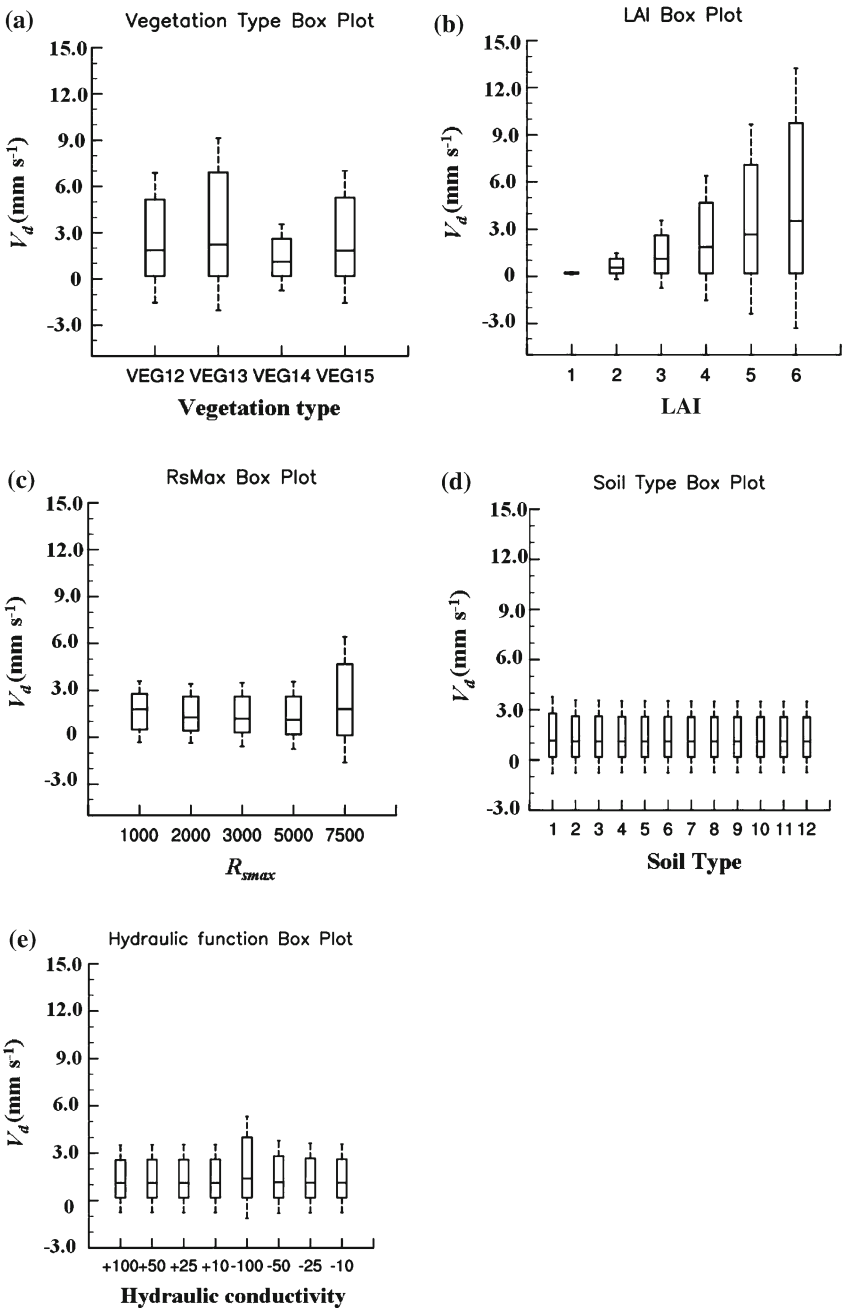

Fig. 6 Box plots for June 2002 dry deposition velocity (V_d) with different parameter changes: **a** vegetation type, **b** leaf area index, **c** maximum stomatal resistance (R_{smax}, s m^{-1}), **d** soil texture, and **e** hydraulic function over the Niwot Ridge study site. The *solidline* is observations. *Dashedline* corresponds to model results. Soil types were classified as (1) sand, (2) loamy sand, (3) sandy loam, (4) silt loam, (5) silt, (6) loam, (7) sandy clay loam, (8) silty clay loam, (9) clay loam, (10) sandy clay, (11) silty clay, and (12) clay. VEG 12 refers to the deciduous needle leaf forest; VEG13 refers to the evergreen broadleaf forest; VEG14 refers to the evergreen needle leaf forest; VEG15 refers to the mixed forest

0.0–4.0 mm s^{-1} respectively. The V_d values were highly sensitive to leaf area index prescription (Fig. 6b). Lower LAI values resulted in smaller V_d values, which were expected since the R_c in the model was estimated by scaling it with LAI values of each vegetation type. Therefore, higher LAI leads to lower total R_c values (not shown) and higher V_d values.

Figure 6c shows the sensitivity of V_d to R_{smax}, which is currently an arbitrary constant in the Noah model based on Noilhan and Planton (1989). The R_{smax} value directly affects the nighttime R_c and hence $V_d$values. Interestingly, the R_{smax} specification also affects the daytime R_c due to impacts on the maximum photosynthesis rate calculation in the GEM model and the F1 term (a function of the amount of photosynthetically-active radiation in the Jarvis type R_c scheme in the default Noah). The V_d (and R_c) values ranged from 1–4 mm s^{-1} to 2–7 mm s^{-1} (from 2,000–7,500 s m^{-1}) as seen in Fig. 6c, consistent with previous studies using other V_d models. For example, Walmsley and Wesely (1996); Finkelstein et al. (2000) and Pleim et al. (2001) found a similar sensitivity to LAI and R_{smax} in the Wesely deposition scheme.

Uncertainties in the soil texture had little impact on V_d values (Fig. 6d), and even with the extreme change in soil texture from clay to sand, there was little impact on the model results. Examining the average diurnal plots (not shown) reveals that the effect was noticeable only during the late afternoon. Modelled V_d values were somewhat sensitive to both the hydraulic function (Fig. 6e) and maximum soil moisture content (particularly when it was reduced, results not shown). However, many other parameters caused no significant changes in V_d values (figures not shown): albedo, emissivity, surface roughness, green vegetation fraction, dry soil moisture content, reference soil moisture content, saturated soil hydraulic conductivity, saturated soil water diffusivity, soil moisture wilting point at which transpiration ceases, and quartz content.

A number of studies, e.g. Noilhan and Planton (1989); Pleim AND Xiu (1995); Chen et al. (1996); Betts et al. (1997); Niyogi et al. (1999), identified LAI and vegetation fraction as first-order parameters that affect the land-surface model performance, particularly when reviewing surface energy fluxes. Our study also identified that both LAI and vegetation fraction have a dominant impact on latent heat flux (figure not shown), but only LAI had a significant impact on $V_d$values. Similarly, when considering the effect of soil texture, sand and loamy sand caused the lowest latent heat fluxes. This was due to the corresponding changes in soil parameters such as hydraulic function and saturated soil hydraulic conductivity. There was, however, a limited impact on V_d values as discussed earlier.

The impact of soil moisture on V_d was examined next (figure not shown). Soil moisture is a prognostic variable and the model system was run for several months to eliminate the memory of the initial conditions. Therefore, it is impossible to see the effect of initial soil moisture on the model results. Instead, we reviewed the relationships between coincident soil moisture and V_d, (Fig. 7) and latent heat flux and V_d at 1400 LT each day for June 2002 (Figure not shown). Latent heat flux and V_d values only showed a better correlation under low LAI conditions (cf. Pleim et al. 1999). The V_d value and soil moisture also correlated well at the lower LAI values. As expected, V_d and R_c correlated well regardless of changes in vegetation types, *LAI*, or R_{smax} (Fig. 8). Reviewing these results, we concluded that the major parameters affecting V_d (and R_c) are vegetation type, *LAI*, soil texture, and R_{smax}.

3.3 Factorial Analysis

Building on the results of the one-at-time sensitivity testing, the impacts of multiple variable changes and interactions were analysed next. For this we used a factorial based Pareto analysis (Haaland 1989; Niyogi et al. 1999). Pareto plots are graphical representations of

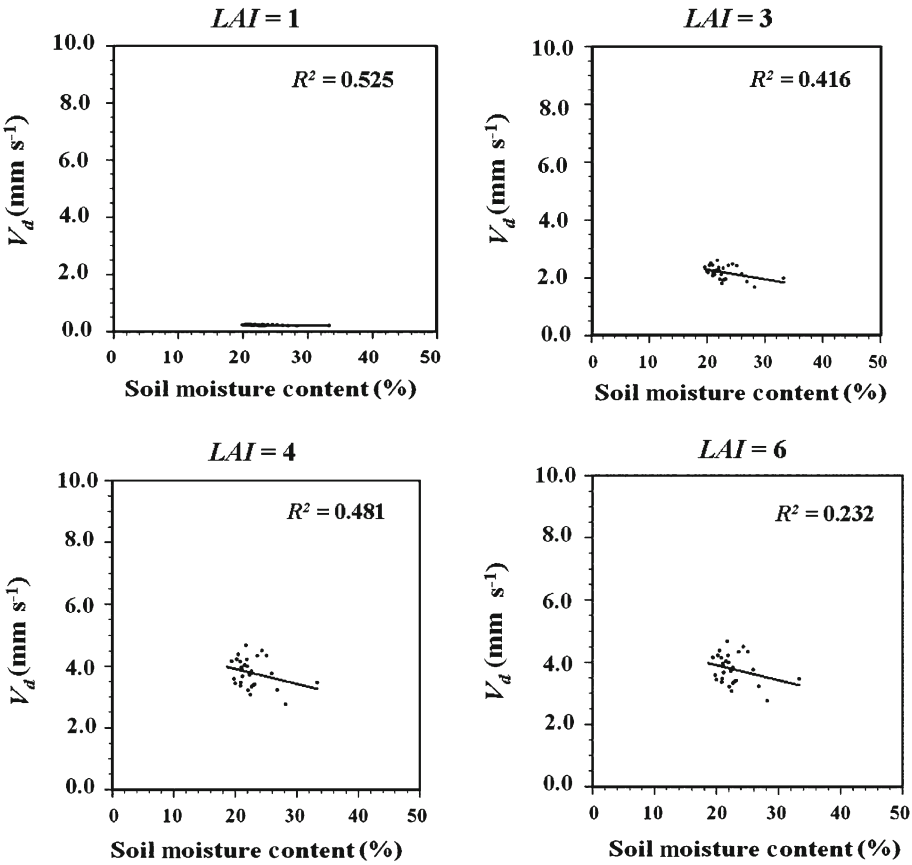

Fig. 7 Scatter plots of dry deposition velocity (V_d) and soil moisture content for different LAI values from 1 to 6, for June 2002 at 1400 LT

the direct (main) effects and the interaction terms between the model variables or between input parameters (e.g. Fig. 9). Pareto plots consist of bar graphs that display a percentage of the sum of mean squares of the effect (V_d in this case), and a line graph that presents the cumulative percentage for each category. Figure 9 shows a pareto plot for the model runs corresponding to four variables: *LAI*, vegetation type, R_{smax}, and soil texture (from Table 1).

In the plot, the bars for leaf area index and vegetation type (*Veg*) present the individual effects while the bars corresponding to *Veg:LAI* represent the interaction effect between vegetation type and leaf area index. The size of the bar is an indication of the sensitivity of the effect. For example in Fig. 9a, b, *LAI* is the dominant term affecting the simulation for both wet (7–12 June 2002) and dry conditions (23–30 June 2002). Additionally the model V_d results show a secondary dependence on vegetation types (*Veg*) and vegetation type interaction with leaf area index (*Veg:LAI*). Interactions of maximum stomata resistance (R_{smax}) and maximum stomata resistance with leaf area index ($R_{smax} : LAI$) were the next most important factors affecting V_d sensitivity. After removing *LAI* as an independent factor, R_{smax} became the dominant variable affecting V_d variations. The pareto analysis, thus, highlights the significance of *LAI* and R_{smax} as the two most important terms affecting the model's V_d values.

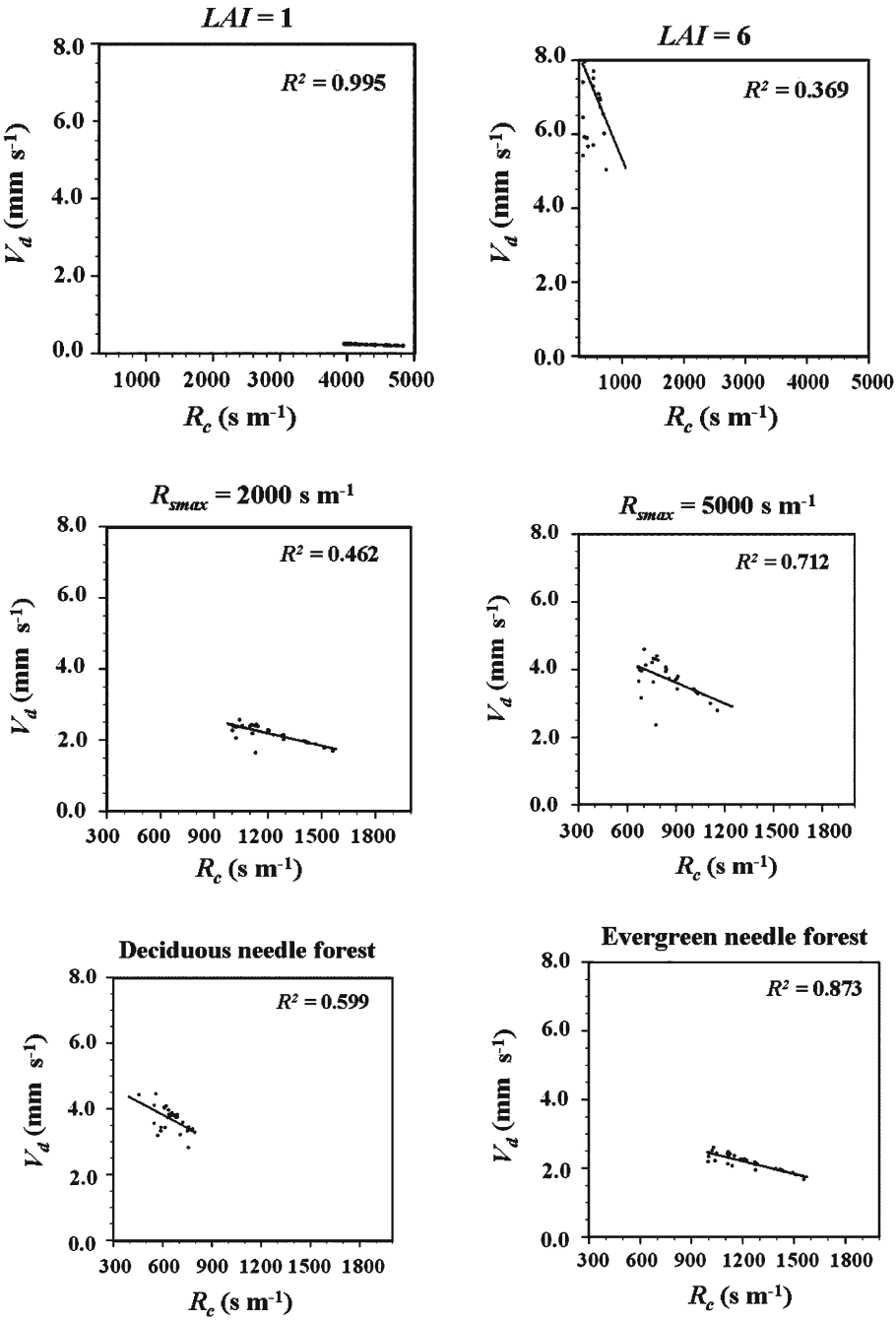

Fig. 8 Scatter plots of dry deposition velocity (V_d) and canopy resistance (R_c) for different LAI, maximum stomata resistance (R_{smax}) and vegetation types for June 2002 at 1400 LT

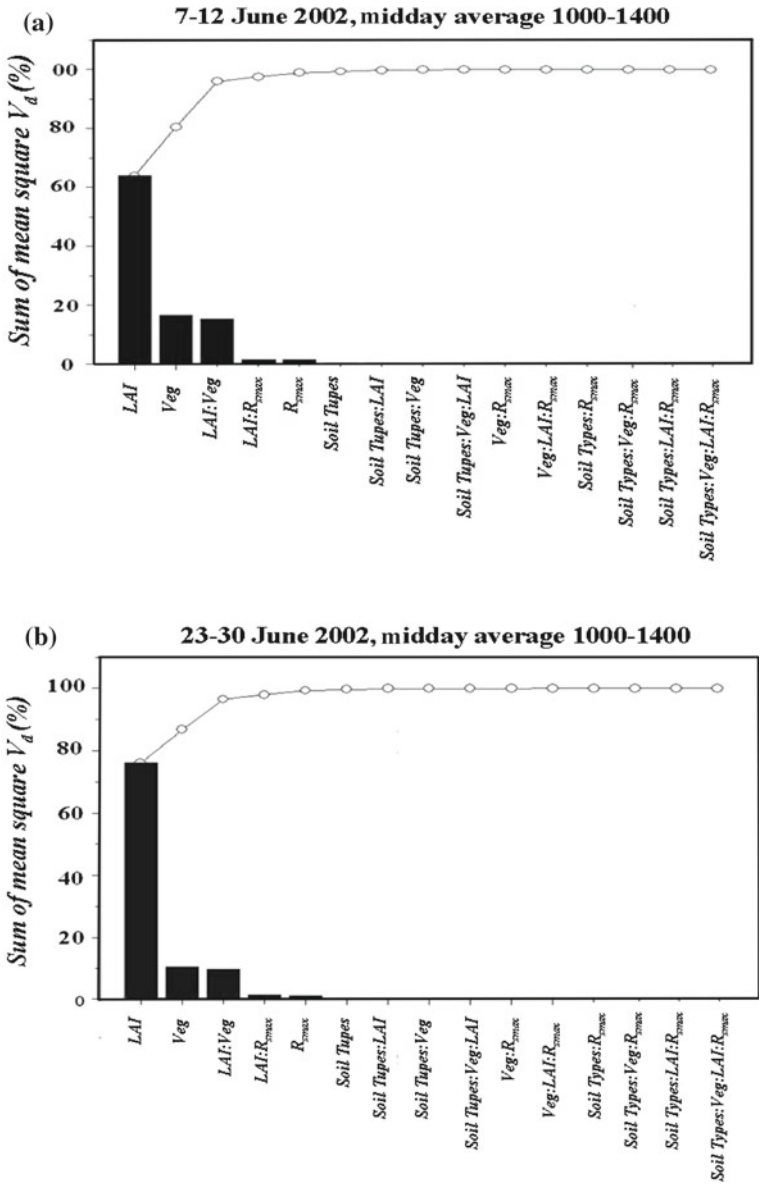

Fig. 9 Pareto plots of the sum of the square of the dry deposition velocity, V_d (%), for different values of leaf area index, vegetation type (*Veg*), maximum stomatal resistance (R_{smax}), and soil textures for **a** 7–12 June 2002 (relatively wet) and **b** 23–30 June 2002 (relatively dry) periods

3.4 Two-Factor Interaction Analysis

The two-factor interaction analysis (TFI) illustrates more explicitly the interactions identified in the Pareto analysis. TFI uses two-way analysis of variance (ANOVA) to calculate the significance of the two factors and their interaction. In the TFI plot, the slopes of the lines

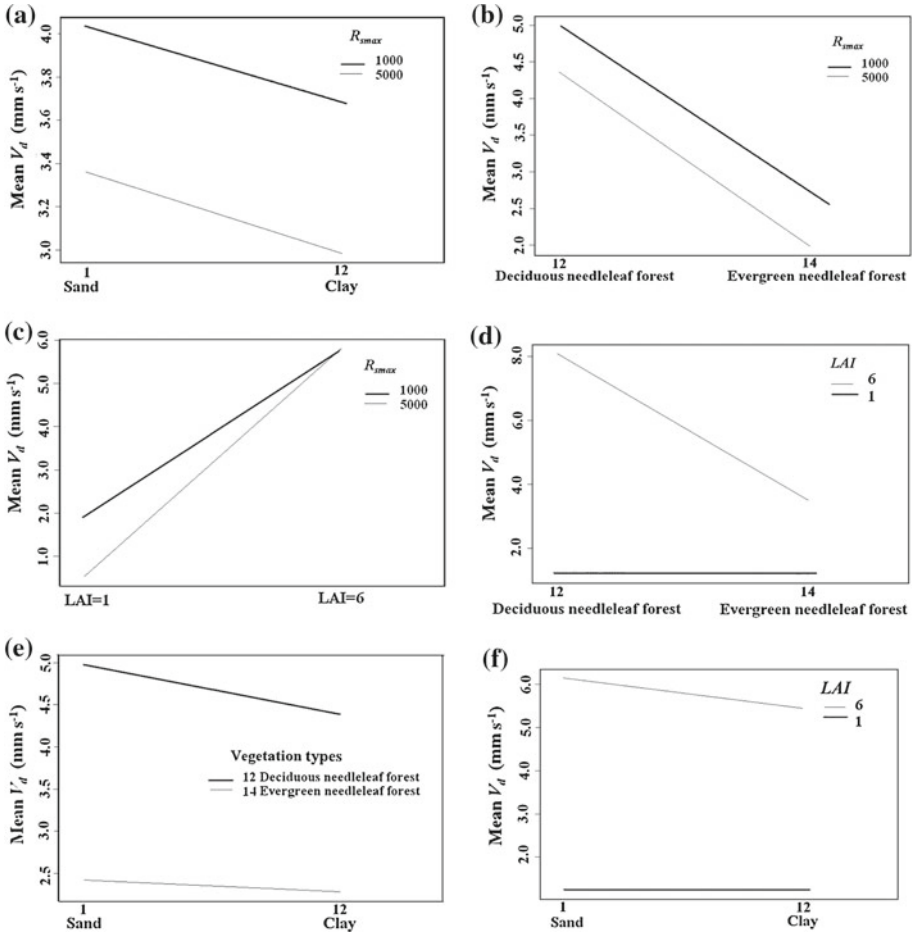

Fig. 10 Interaction plots of dry deposition velocity (V_d) with **a** maximum stomatal resistance (R_{smax}) and soil texture, **b** with R_{smax} and vegetation type, **c** with R_{smax} and leaf area index, **d** with *LAI* and vegetation type, **e** with vegetation type and soil texture, and **f** with *LAI* and soil texture for 7–12 June 2002

for different variable settings provide information regarding the sensitivity of a variable in the model (Niyogi et al. 1999). Thus, the interpretation of the results depends on the slope of the interaction plots. Figure 10 shows the TFI plots for R_{smax}, vegetation type, and soil texture (cf. Fig. 9). In Fig. 10a, b, the R_{smax} and vegetation type interaction, as well as the R_{smax} and soil texture interaction, results in parallel lines. This suggests a limited interaction between the two parameters when estimating V_d values. On the other hand, Fig. 10c shows that the two lines of R_{smax} and *LAI* are not parallel and indicate a high degree of interaction. In particular, as the two lines show a larger difference at lower LAI values, this indicates a high sensitivity of R_{smax} at lower *LAI*. Similarly, when reviewing the slopes for R_{smax} lines, the slope for higher R_{smax} suggests that the sensitivity of *LAI* to V_d estimation is higher for higher R_{smax} slopes. The interaction terms also show higher sensitivity of vegetation type for higher *LAI*. Similarly, Fig. 10d shows that the sensitivity and uncertainty of V_d are more pronounced for deciduous needle leaf when compared to evergreen needle leaf forest,

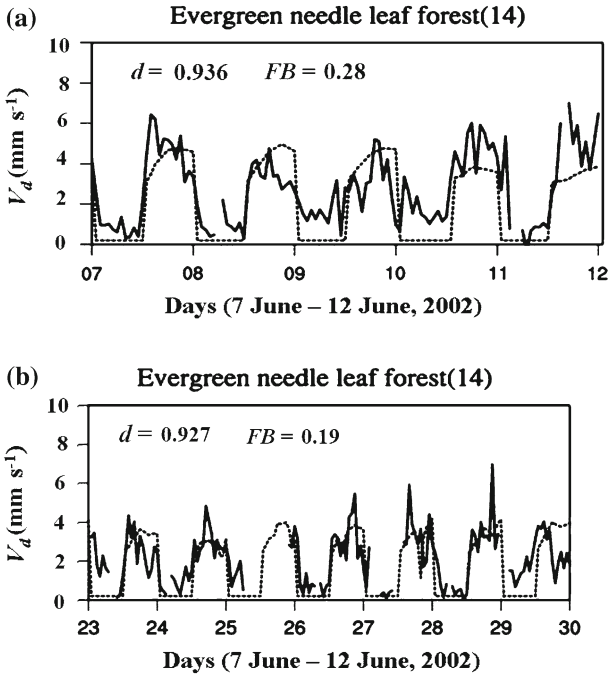

Fig. 11 Dry deposition velocity (V_d) time series plots for **a** 7–12 June 2002 with the $LAI = 4.2$ and **b** 23–30 June 2002 with the $LAI = 3.8$. Observed V_d ($solidline$) and modelled V_d ($dashedline$) over evergreen needle leaf forest (14) during wet period, 7–12 June 2002 and dry period, 23–30 June 2002. The variable, d, is the index of agreement and FB is the fractional bias (mm s^{-1})

as the LAI increases (Fig. 10d). Figure 10e and f shows minor interaction effects between vegetation type and LAI as a function of soil texture. The interactions between LAI, R_{smax}, vegetation types, and soil textures impacting V_d were relatively insensitive to soil moisture (figure not shown). Again, when compared to surface energy fluxes, the V_d results appear to be, generally, only sensitive to LAI, R_{smax}, and vegetation type specification.

3.5 Model Modifications

The sensitivity analysis indicates that LAI and R_{smax} appear to be the critical variables affecting V_d estimates. Therefore, the default LAI value was modified to reflect the canopy phenological changes over the study site that have been observed when $LAI = 4.2$. The resulting model performance showed better agreement for the wet period when $LAI = 4.2$ and for the dry period when $LAI = 3.8$ (Fig. 11). This outcome highlights a need for assimilating variable LAI/normalized difference vegetation index (NDVI) or having dynamic LAI within the model for future work. During the dry period, the decreased V_d may not be directly caused by reduced LAI. Rather, it might have been due to soil moisture conditions, which control maximum catalytic rubisco capacity (V_{max}) for calculating R_c. Consequently, another variable, R_{smax}, was tested by reducing the current default value. Tests with a range of observed values suggested that a value of 1,250 s m^{-1} during the wet period and 1,700 s m^{-1} during the dry period produced the best results, corresponding to increased V_d values during nighttime (Fig. 12). Future efforts should be directed towards additional improvements for nighttime

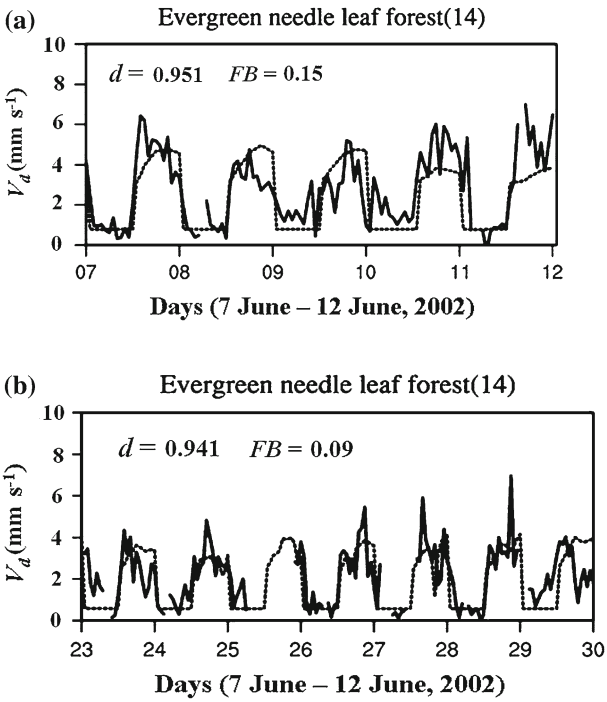

Fig. 12 Dry deposition velocity (V_d) time series plots for **a** 7–12 June 2002 (relatively wet) period with the $LAI = 4.2$ and the R_{smax} of 1,250 s m^{-1} **b** for 23–30 June 2002 (relatively dry) period, with the $LAI = 3.8$ and the R_{smax} of 1, 700 s m^{-1}. Observed V_d (*solidline*) and modelled V_d (*dashedline*). The variable, *d*, is the index of agreement and *FB* is the fractional bias (mm s^{-1})

R_c by considering radiation, hydraulic conductivity, vapour pressure deficit, leaf age, and canopy turbulence (Snyder et al. 2003; Bucci et al. 2003; Daley and Phillips 2006; Kavanagh et al. 2007; Mairgareth et al. 2007; Turnipseed et al. 2009).

3.6 Further Performance Test

To further demonstrate the positive impact of the changes recommended in *LAI* and R_{smax}, we applied the model over two different sites: Bondville, Illinois (agriculture site) and Duke Forest (needle leaf site). At both these locations, only energy flux observations were available for verification. The model was run with four configurations: (i) default, (ii) change in leaf area index with a higher value for the wet period and lower value for the dry period, (iii) with lower R_{smax} values, and (iv) by changing both the leaf area index and R_{smax}. The *LAI*, R_{smax} changes were linked to the soil conditions (*SMC* in Eq. 4).

$$Corrected\ LAI = \frac{LAI}{(0.95 + (0.1SMC))}, \tag{3}$$

$$SMC = \frac{W_2 - W_{wilt}}{W_{\max} - W_{wilt}}, \tag{4}$$

where *LAI* is leaf area index, W_2 is the deep soil moisture content (m^3 m^{-3}), W_{wilt} is the wilting point soil moisture (m^3 m^{-3}), and W_{max} is the maximum soil moisture content (m^3 m^{-3}).

Table 2 Summary of the fractional bias ($W\,m^{-2}$) of sensible heat flux (*H*) and latent heat flux (*LE*) over Duke Forest and Bondville study sites

Runs	Duke forest		Bondville	
	H bias ($W\,m^{-2}$)	*LE* bias ($W\,m^{-2}$)	*H* bias ($W\,m^{-2}$)	*LE* bias ($W\,m^{-2}$)
Default	−0.304	0.206	−0.314	0.123
Obs-Both_correct	−0.287	0.182	−0.294	0.105
Obs-corrected LAI	−0.288	0.186	−0.300	0.112
Obs-corrected R_{smax}	−0.303	0.202	−0.308	0.116

Obs is observed data. Both_correct indicates *LAI* and R_{smax} have been corrected; corrected LAI:*LAI* has been corrected and corrected R_{smax}:R_{smax} has been corrected

The new parameter values were estimated using

$$LAI = LAI/LAI_{corr}, \tag{5}$$

$$Corrected R_{smax} = \frac{R_{smax}}{LAI/LAI_{corr}}, \tag{6}$$

where LAI_{corr} is the corrected LAI. Using these equations, the leaf area index was set from 4 to 4.12 for the Duke Forest site and from 4 to 4.19 for the Bondville site. The R_{smax} ranged from 1,214 to 1,232 s m^{-1} for Duke Forest and from 1,194 to 1,218 s m^{-1} for Bondville. Results showed small differences but overall positive improvements in the model performance as summarized in Table 2.

4 Conclusions

The deposition velocity estimation capability of the Noah/HRLDAS model, based on a photosynthesis-based canopy resistance model (GEM), was evaluated with observations from a conifer forest at the Niwot Ridge AmeriFlux site, Colorado, USA. The observations and model results were analysed and compared for two different periods, 7–12 June 2002 (relatively wet soil) and 23–30 June 2002 (relatively dry soil). Using the default $LAI = 4$, the model performed well for wet to moderately wet soil conditions but slightly overestimated V_d for the dry period. In general, the model simulates the daytime variation of V_d but has difficulty in treating the nighttime canopy and aerodynamic resistances. A large number (112) of model experiments were conducted for testing the sensitivity of the model to different soil and vegetation parameters, and showed that the V_d estimation was mostly sensitive to the *LAI* and R_{smax} prescription. Vegetation type had a modest impact as did soil moisture and soil texture specifications. Soil and vegetation parameters such as soil texture and vegetation fraction had a larger impact on the latent heat flux estimation than on V_d estimates. Our results suggest that the Noah land-surface model performance can be improved by changing both the specifications of LAI dynamics or phenology and the R_{smax} prescription. Additional experiments were performed by changing *LAI* and R_{smax}. Our results showed that the GEM-Noah-HRLDAS model's framework can be effectively applied to estimate deposition velocity values for air quality/biogeochemical studies, particularly when land-surface conditions are accurately prescribed.

We recommend that future improvements of the Noah LSM should focus on including the assimilation of NDVI data and incorporating a dynamic LAI estimation into the

deposition and canopy resistance model. Additionally, it was noted that the R_{smax} specification within the Noah model needs further evaluation based on recent studies that suggest nighttime transpiration of each species (Synder et al. 2003).

Acknowledgments This research benefited through the NOAA/JCSDA grant (NA06NES4400013), NCAR BEACHON (Bio-hydro-atmosphere interactions of Energy, Aerosols, Carbon, H_2O, and Organics & Nitrogen) Program, NASA Terrestrial Hydrology Program (Dr. Jared Entin), and NSF CAREER (Drs. Liming Zhou and Jay Fein). It was also supported by the National Natural Science Foundation of China (NSFC Grant No. 40875076). The observation data from NWR AmeriFlux sites has been provided by Dr. Russ Monson (http://public.ornl.gov/ameriflux/Site_Info/siteInfo.cfm?KEYID=us.niwot_ridge.01).

Appendix A: Deposition Velocity Algorithm

A simplified dry deposition velocity (V_d) module is considered in the HRLDAS. V_d is estimated from the aerodynamic resistance (R_a), the laminar boundary-layer resistance (R_b) and the canopy resistance (R_c) (Wesely 1989) as,

$$V_d = (R_a + R_b + R_c)^{-1}, \tag{7}$$

while the aerodynamic resistance (R_a) is calculated as a function of wind speed (m s^{-1}) (Lui et al. 2007).

$$R_a = 94.909u^{-0.9036} \tag{8}$$

The boundary-layer resistance (R_b) is derived following Nikolov et al. (1995), as used by Niyogi et al. (2003) for free convection (R_{bfc}) and forced convection (R_{bfr}) conditions,

$$\frac{1}{R_{bfc}} = cT^{0.56}\left[(T + 120)\frac{u}{Pd}\right]^{0.5}, \tag{9}$$

$$\frac{1}{R_{bfr}} = cT_s^{0.56}\left\{\frac{T_s + 120}{P}\right\}^{0.5}\left\{\frac{T_{vs} - T_{va}}{d}\right\}^{0.25}. \tag{10}$$

In the above, T is the air temperature (in kelvin, K), T_s is the surface temperature, while T_{vs} and T_{va} are virtual surface and virtual air temperatures (K); u is the wind speed (m s^{-1}), P is the pressure (Pa), and d is the leaf length scale (m); c is a scaling constant that equals 4.322×10^{-3} for broad leaves and 1.203×10^{-3} for conifers (Nikolov et al. 1995).

The canopy resistance (R_c) is considered the primary resistance term to estimate V_d and is assumed to include both the stomatal and non-stomatal processes. The R_c term in the Noah-GEM model is calculated from the Ball–Berry approach (Ball et al. 1987) as

$$1/R_c = m\frac{A_n}{C_s}h_s + b, \tag{11}$$

where A_n (mol m^{-2} s^{-1}) is the photosynthesis rate, h_s (%) is the relative humidity at the canopy surface, and C_s (mol m^{-3})is the CO_2 concentration at the canopy surface. The terms m and b are the species-specific gas exchange constants. Details regarding the formulations and constants can be found in Niyogi et al. (2003, 2006, 2009). The photosynthesis rate (A_n) depends on three main factors: the rubisco limitation (W_c), the amount of photosynthetically-active radiation (W_e), and the capacity of the C3 vegetation to utilize the photosynthesis products or the phophoenolpyruvate carboxylase limitation in C4 vegetation (W_s). The terms W_c and W_s are a function of the maximum catalytic rubisco capacity for the

leaf (V_m) derived from temperature and soil moisture. The W_e term is a function of radiation, CO_2 concentration, and the CO_2 compensation point.

References

Alfieri JG, Niyogi D, Blanken PD, Chen F, LeMone MA, Mitchell KE, Ek MB, Kumar A (2008) Estimation of the minimum canopy resistance for croplands and grasslands using data from the 2002 International H2O Project. Mon Weather Rev 136:4452–4469

Baldocchi DD, Hicks BB, Camara P (1987) A canopy stomatal resistance model for gaseous deposition to vegetated surfaces. Atmos Environ 21:91–101

Ball J, Woodrow I, Berry J (1987) A model predicting stomatal conductance and its contribution to the control of photosynthesis under different environmental conditions. Prog Photosynth Res 4:221–224

Betts R, Cox P, Lee S, Woodward F (1997) Constrating physiological and structural vegetation feedbacks in climate change simulations. Nature 387:796–799

Bucci SJ, Scholz FG, Goldstein G, Meinzer FC, Sternberg LSL (2003) Dynamic changes in hydraulic conductivity in petioles of two savanna tree species: factors and mechanisms contributing to the refilling of embolized vessels. Plant Cell Environ 26:1633–1645

Cavender-Bare J, Sack L, Savage J (2007) Atmospheric and soil drought reduce nocturnal conductance in live oaks. Tree Physiol 27:611–620

Chen F, Dudhia J (2001) Coupling an advanced land surface–hydrology model with the Penn State–NCAR MM5 modelling system. Part I: model implementation and sensitivity. Mon Weather Rev 129:569–585

Chen F, Mitchell K, Schaake J, Xue Y, Pan H, Koren V, Duan Y, Ek M, Betts A (1996) Modelling of land-surface evaporation by four schemes and comparison with FIFE observations. J Geophys Res 101:7251–7268

Chen F, Manning KW, LeMone MA, Trier SB, Alfieri JG, Roberts R, Tewari M, Niyogi D, Horst TW, Oncley SP, Basara JB, Blanken PD (2007) Description and evaluation of the characteristics of the NCAR high-resolution land data assimilation system. J Appl Meteorol Climatol 46:694–713

Cooter EJ, Schwede D (2000) Sensitivity of the national oceanic and atmospheric administration multiplayer model to instrument error and parameterization uncertainty. J Geophys Res 105:6695–6704

Daley MJ, Phillips NG (2006) Interspecific variation in nighttime transpiration and stomatal conductance in a mixed New England deciduous forest. Tree Physiol 26:411–419

Ek MB, Mitchell KE, Lin Y, Rogers E, Grunmann P, Koren V, Gayno G, Tarpley JD (2003) Implementation of Noah land surface model advances in the national centers for environmental prediction operational mesoscale eta model. J Geophys Res 108:8851

Erisman JW, van Pul A, Wyers P (1994) Parameterization of surface resistance for the quantification of atmospheric deposition of acidifying pollutants and ozone. Atmos Environ 28:2595–2607

Finkelstein PL, Ellestad TG, Clarke JF, Meyers TP, Schwede DB, Hebert EO, Neal JA (2000) Ozone and sulfur dioxide dry deposition to forests: observations and model evaluation. J Geophys Res 105:365–377

Fisher JB, Baldocchi DD, Mission L, Dawson TE, Goldstein AH (2007) What the towers don't see at night: nocturnal sap flow in trees and shrubs at two AmeriFlux sites in California. Tree Physiol 27:597–610

Fulton RA, Breidenbach JP, Seo DJ, Miller DA, Bannon TO (1998) The WSR-88D rainfall algorithm. Weather Forecast 13:377–395

Garland JA, Atkins DHF, Readings CJ, Caughey SJ (1974) Deposition of sulphur dioxide to the ground. Atmos Environ 8:75–79

Grell AG, Peckham SE, Schmitz R, McKeen SA, Frost G, Skamarock WC, Eder B (2005) Fully coupled "Online" Chemistry within the WRF model. Atmos Environ 39:6957–6975

Haaland PD (1989) Experimental design in biotechnology. Marcel Dekker Inc., New York, 105 pp

Hicks BB, Baldocchi DD, Hosher RP, Hutchison BA, Matt Dr, McMillen RT, Satterfield LC (1985) On the use of monitor air concentrations to infer dry deposition. NOAA technical memorandum ERLO ARLZ141, 65 pp

Hicks BB, Baldocchi DD, Meyers TP, Hosker RP, Matt DR (1987) A preliminary multiple resistance routine for deriving dry deposition velocities from measurement quantities. Water Air Soil Pollut 36:311–330

Kavanagh KL, Pangle R, Schotzko A (2007) Nocturnal transpiration causing disequilibrium between soil and stem predawn water potential in mixed conifer forests of Idaho. Tree Physiol 27:621–629

Kumar A, Chen F, Niyogi D, Manning K, Mitchell K, Ek M, Alfieri JG (2008) Integrating a photosynthesis-based canopy resistance model and satellite data in Noah land surface model. AMS. http://ams.confex.com/ams/pdfpapers/131425.pdf. Accessed 20 January 2008

Lamaud E, Carrara A, Brunet Y, Lopez A, Druilhet A (2002) Ozone fluxes above and within a pine forest canopy in dry and wet conditions. Atmos Environ 36:77–88
Lui S, Mao D, Jia L (2007) Evaluating parameterizations of aerodynamic resistance to heat transfer using field measurements. Hydrol Earth Syst Sci 11:769–783
Mairgareth AC, Richards JH, Donovan LA (2007) Conductance and transpiration in C3 and C4 plants. Plant Physiol 143:4–10
Meyers TP, Finkelstein P, Clarke J, Ellestad TG, Sims PF (1998) A multilayer model for inferring dry deposition using standard meteorological measurements. J Geophys Res 103:645–661
Muller JF, Stavrakou T, Wallens S, Smedt ID, Roozendael MV, Potosnak MJ, Rinne J, Munger A, Goldstein A, Guenther AB (2008) Global isoprene emissions estimated using MEGAN, ECMWF analyses and a detailed canopy environment model. Atmos Chem Phys 8:1329–1341
Musselman CR, Minnick TJ (2000) Nocturnal stomata conductance and ambient air quality standards for ozone. Atmos Environ 34:719–733
Nikolov N, Massman W, Schoettle A (1995) Coupling biochemical and biophysical processes at the leaf level: an equilibrium photosynthesis model for leaves of C3 plants. Ecol Model 80:205–235
Niyogi D, Raman S (1997) Comparison of four different stomatal resistance schemes using FIFE observations. J Appl Meteorol 36:903–917
Niyogi D, Xue YK (2006) Soil moisture regulates the biological response of elevated atmospheric CO2 concentrations in a coupled atmosphere biosphere model. Glob Planet Chan 54:94–108
Niyogi D, Raman S, Alapaty K (1999) Uncertainty in specification of surface characteristics, part 2: hierarchy of interaction explicit statistical analysis. Boundary-Layer Meteorol 91:341–366
Niyogi D, Raman S, Alapaty K (2003) A photosynthesis-based dry deposition modelling approach. Water Air Soil Pollut 144:171–194
Niyogi D, Alapaty K, Phillips S, Aneja V (2006) Considering ecological formulations for estimating deposition velocity in air quality models. Int J Glob Environ 6:270–284
Niyogi D, Alapaty K, Raman S, Chen F (2009) Development and evaluation of a coupled photosynthesis-based gas exchange evapotranspiration model (GEM) for mesoscale weather forecasting applications. J Appl Meteorol Climatol 48:349–368
Noilhan J, Planton S (1989) A simple parameterization of land surface processes for meteorological models. Mon Weather Rev 117:536–549
Pleim JE, Xiu A (1995) Development and testing of a surface flux planertary boundary layer model with explicit soil moisture parameterization for applications in mesoscale models. J Appl Meteorol 34:16–32
Pleim JE, Finkelstein PL, Clarke JF, Ellestad TG (1999) A technique for estimating dry deposition velocities based on similarity with latent heat flux. Atmos Environ 33:2257–2268
Pleim JE, Xiu A, Finkelstein PL, Otte TL (2001) A coupled land-surface and dry deposition model and comparison to field measurements of surface heat, moisture, and ozone fluxes. Water Air Soil Pollut 1:243–252
Snyder KA, Richards JH, Donovan LA (2003) Night-time conductance in C3 and C4 species: do plants lose water at night? J Exp Bot 54:861–865
Turnipseed AA, Anderson DE, Blanken PD, Baugh WM, Monson RK (2003) Airflows and turbulent flux measurements in mountainous terrain: part 1 canopy and local effects. Agric For Meteorol 119:1–21
Turnipseed AA, Huey LG, Nemitz E, Stickel R, Higgs J, Tanner DJ, Slusher DL, Sparks JP, Flocke F, Guenther A (2006) Eddy covariance fluxes of peroxyacetylnitrates (PANs) and NOy to a coniferous forest. J Geophys Res 11:1–17
Turnipseed AA, Burns S, Moore D, Hu J, Guenther A, Monson R (2009) Controls over ozone deposition to a high elevation subalpine forest. Agric For Meteorol 149:1446–1459
Walmsley JL, Wesely ML (1996) Modification of coded parameterizations of surface resistances to gaseous dry deposition. Atmos Environ 30:1181–1188
Wesely ML (1989) Parameterization of surface resistance to gaseous dry deposition in regional scale numerical models. Atmos Environ 23:1293–1304
Wesely ML, Hicks BB (1977) Some factors that affect the deposition rates of sulfur dioxide and similar gases on vegetation. J Air Pollut Control Assoc 27:110–1116
Wu Y, John W, Donna S, Peters-Lidard C, Dennis R, Robarge W (2009) A new model of bi- directional ammonia exchange between the atmosphere and biosphere: ammonia stomatal compensation point. Agric For Meteorol 149:263–280
Zhang L, Brook JR, Vet R (2003) A revised parameterization for gaseous dry deposition in air quality models. Atmos Chem Phys 3:2067–2082